Molecular Biology of the Cell
Vol. 13, 2718–2731, August 2002

The Microtubule-destabilizing Kinesin XKCM1 Regulates Microtubule Dynamic Instability in Cells

Susan L. Kline-Smith* and Claire E. Walczak†‡

Departments of *Anatomy and Cell Biology and †Biochemistry and Molecular Biology, Indiana University Medical Sciences Program, Bloomington, Indiana 47405

Submitted December 6, 2001; Revised May 6, 2002; Accepted May 23, 2001
Monitoring Editor: Ted Salmon

The dynamic activities of cellular microtubules (MTs) are tightly regulated by a balance between MT-stabilizing and -destabilizing proteins. Studies in *Xenopus* egg extracts have shown that the major MT destabilizer during interphase and mitosis is the kinesin-related protein XKCM1, which depolymerizes MT ends in an ATP-dependent manner. Herein, we examine the effects of both overexpression and inhibition of XKCM1 on the regulation of MT dynamics in vertebrate somatic cells. We found that XKCM1 is a MT-destabilizing enzyme in PtK2 cells and that XKCM1 modulates cellular MT dynamics. Our results indicate that perturbation of XKCM1 levels alters the catastrophe frequency and the rescue frequency of cellular MTs. In addition, we found that overexpression of XKCM1 or inhibition of KCM1 during mitosis leads to the formation of aberrant spindles and a mitotic delay. The predominant spindle defects from excess XKCM1 included monoastral and monopolar spindles, as well as small prometaphase-like spindles with improper chromosomal attachments. Inhibition of KCM1 during mitosis led to prometaphase spindles with excessively long MTs and spindles with partially separated poles and a radial MT array. These results show that KCM1 plays a critical role in regulating both interphase and mitotic MT dynamics in mammalian cells.

INTRODUCTION

Microtubules (MTs) are cytoskeletal polymers comprised of α- and β-tubulin heterodimers. Their head-to-tail arrangement within the MT confers structural polarity to the polymer. The radial array of MTs in an interphase cell is largely organized by the centrosome, with the MT minus ends at the centrosome and the plus ends extending out toward the cell periphery. MTs exhibit a behavior termed dynamic instability, wherein a population of MTs, whether in vitro or in vivo, contains both growing and shrinking polymers that interconvert infrequently and randomly between these two states (Mitchison and Kirschner, 1984). MT dynamics can be described by four parameters: growth rate; shrinkage rate; catastrophe frequency, which is the transition from growth to shrinkage; and rescue frequency, which is the transition from shrinkage to growth (Walker *et al.*, 1988). MT turnover in vivo is much greater than in solutions of pure tubulin (for review, see Desai and Mitchison, 1997), suggesting the presence of cellular factors that regulate MT dynamics. One of the most striking examples of cellular regulation of MT dynamics is the sudden increase in MT turnover upon the transition from interphase to mitosis (Salmon *et al.*, 1984; Saxton *et al.*, 1984), which results in a decrease in total MT polymer levels at the beginning of mitosis (Zhai *et al.*, 1996). Overall, mitotic MTs are more dynamic than interphase MTs; astral MTs associated with the mitotic spindle exhibit an increase in the catastrophe frequency and a decrease in the rescue frequency of MTs in cultured cells (Rusan *et al.*, 2001).

Numerous studies have shown that the interphase MT array is tightly regulated by the opposing activities of MT stabilizers, commonly known as MT-associated proteins (MAPs), and MT destabilizers, such as Op18 or the kinesin-related protein *Xenopus* kinesin catastrophe modulator-1 (XKCM1) (for review, see Cassimeris and Spittle, 2001). XKCM1 belongs to a group of kinesins that regulate aspects of MT dynamics during mitosis (Endow *et al.*, 1994; Walczak *et al.*, 1996; Cottingham and Hoyt, 1997; Desai *et al.*, 1999; Maney *et al.*, 2001; Severin *et al.*, 2001; West *et al.*, 2001). Inactivation of XKCM1 in mitotic *Xenopus* egg extracts results in huge asters of long, nondynamic MTs that are incapable of forming a mitotic spindle. Measurement of MT dynamics revealed that XKCM1 inhibition leads to a fourfold decrease in the catastrophe frequency in mitotic egg extracts (Walczak *et al.*, 1996). Biochemical analysis showed

Article published online ahead of print. Mol. Biol. Cell 10.1091/mbc.E01–12–0143. Article and publication date are at www.molbiolcell.org/cgi/doi/10.1091/mbc.E01–12–0143.

‡ Corresponding author. E-mail address: cwalczak@indiana.edu.

Abbreviations used: MAP, microtubule-associated protein; MCAK, mitotic centromere-associated kinesin; MT, microtubule; XKCM1, *Xenopus* kinesin catastrophe modulator-1.

that XKCM1 uses the energy derived from ATP hydrolysis to depolymerize MTs rather than to translocate along the MT lattice like conventional kinesins (Desai *et al.*, 1999).

Studies in egg extracts have also shown that XKCM1 plays a role in regulating MT dynamics during interphase, primarily by opposing the activity of the MT stabilizer XMAP215 (Tournebize *et al.*, 2000). In addition, recent studies have demonstrated that in vivo MT dynamics can be reconstituted by combining purified tubulin, XMAP215 and XKCM1 in vitro (Kinoshita *et al.*, 2001). These studies suggest that much of the observed in vivo MT dynamics can be attributed to the antagonizing activities of these two proteins, and that the ability of XKCM1 to depolymerize the interphase MT array is largely inhibited because XMAP215 is bound to MTs. An attractive model is that upon entry into mitosis, XMAP215 transiently dissociates from MTs, allowing XKCM1 to cause an increased number of MT catastrophes (for review, see Heald, 1999; Andersen, 2000).

The experiments to date have examined the activity of XKCM1 by using either purified proteins or *Xenopus* egg extracts comprised of meiotic cytoplasm. The role of XKCM1 in the regulation of MT dynamics in vertebrate somatic cells is not known. A recent study in Chinese hamster ovary (CHO) cells has shown that mitotic centromere-associated kinesin (MCAK), the hamster homolog of XKCM1, destabilizes MTs when overexpressed as a green fluorescent protein (GFP) fusion protein (Maney *et al.*, 2001); however, the changes in MT dynamics that cause this destabilizing effect in cells are unknown.

In this study, we examined the results of both overexpression and inhibition of XKCM1 on MT dynamics in interphase and on spindle morphology during mitosis in PtK2 cells. Our results demonstrate that XKCM1 regulates dynamic instability of cellular MTs, and that the formation and function of the mitotic spindle are perturbed by overexpression of GFP-XKCM1 or by inhibition of KCM1 during mitosis. Our results also suggest that XKCM1 could be used by cells to initiate the increase in MT turnover that occurs when cells enter mitosis and begin formation of the mitotic spindle (for review, see Wittmann *et al.*, 2001).

MATERIALS AND METHODS

Cell Culture

PtK2 cells were grown in minimal essential medium α (MEMα) supplemented with 10% fetal calf serum, penicillin, streptomycin, and L-glutamine (Invitrogen, Carlsbad, CA) in an incubator at 37°C, 5% CO_2. For transfection and immunostaining of interphase cells, cells were plated onto 12-mm glass coverslips at a density of 10,000 cells/cm^2 1 d before transfection. For transfection and immunostaining of mitotic cells, cells were plated at 5000 cells/cm^2 1 d before transfection. To microinject cells in interphase, cells were split 1/4–1/6 2–3 d before injection and plated on 18- × 18-mm or 12-mm glass coverslips depending on the experiment. To microinject cells in prophase, cells were plated onto 12-mm coverslips at 1/6–1/8 3–4 d before injection. For interphase cells that were transfected and subsequently microinjected, cells were grown on 18- × 18-mm glass coverslips at a density of 10,000 cells/cm^2 1 d before transfection.

Preparation of Recombinant GFP-XKCM1

GFP-XKCM1 was created by cloning the full-length cDNA of XKCM1 (Walczak *et al.*, 1996) into the *Sac*I to *Kpn*I sites of pEGFP-C1 (CLONTECH, Palo Alto, CA). The 5′ untranslated region of XKCM1 was removed by polymerase chain reaction. The correct sequence of the clone was verified by sequencing.

Transfection

Transfections were performed using a modified version of a previously published protocol (Heald *et al.*, 1993). Cells were rinsed with fresh media 15–20 min before addition of a mixture containing 5 μg/ml DNA, 13 mM $CaCl_2$, and HEPES-buffered saline (18 mM NaCl, 0.65 mM KCl, 97 μM Na_2HPO_4, 78 μM dextrose, and 3.2 mM HEPES, pH 7.05) in complete media. Cells were returned to the 37°C, 5% CO_2 incubator for 4–5 h then rinsed three times with incomplete MEMα media and covered with complete media. Cells were processed at 24, 48, or 72 h after this time. To enhance the mitotic index of transfected cells, dimethyl sulfoxide was added to fresh media to a final concentration of 0.1% at 24 h posttransfection, and cells were processed for at 72 h posttransfection. This technique was used only for observation of mitotic cells overexpressing GFP or GFP-XKCM1 and never used in any other experiment.

Immunofluorescence

All immunofluorescence labeling procedures were performed at room temperature. Cells were rinsed in phosphate-buffered saline (12 mM phosphate, 137 mM NaCl, and 3 mM KCl, pH 7.4) and fixed for 25 min in BRB-80 [80 mM piperazine-*N*,*N*′-bis(2-ethanesulfonic acid), 1 mM EGTA, and 1 mM $MgCl_2$, pH 6.8] supplemented with 4 mM EGTA, 4% formaldehyde, and 0.01% glutaraldehyde. Free aldehydes were quenched in Tris-buffered saline (TBS) (20 mM Tris and 150 mM NaCl, pH 7.5) plus trace $NaBH_4$ for 5 min. Fixed cells were rinsed with TBS-Triton X-100 (TX) (TBS + 0.1% Triton X-100) and blocked in AbDil (2% bovine serum albumin and 0.1% NaN_3 in TBS-TX) for 20 min. All subsequent rinses between antibody incubations were performed using TBS-TX. All antibodies were diluted in AbDil. For immunofluorescence of MTs, cells were incubated for 20–25 min in 1/500 DM1α (Sigma-Aldrich, St. Louis, MO) followed by a 20–25-min incubation in 1/50 Texas Red-conjugated donkey anti-mouse secondary antibody (Jackson Immuno Research Laboratories, West Grove, PA). For immunofluorescence of XKCM1, cells were incubated for 20–25 min in 5 μg/ml anti-XKCM1-NT (Walczak *et al.*, 1996) followed by a 20–25-min incubation in 1/50 fluorescein-conjugated goat anti-rabbit secondary antibody (Jackson Immuno Research Laboratories). Cells that had been injected with X-rhodamine–labeled tubulin were rinsed with phosphate-buffered saline and fixed for 25 min in PHEM [60 mM piperazine-*N*,*N*′-bis(2-ethanesulfonic acid), 25 mM HEPES, 10 mM EGTA, and 2 mM $MgCl_2$, pH 6.9] supplemented with 4% formaldehyde, 4 mM EGTA, and 0.5% glutaraldehyde. Free aldehydes were quenched in TBS (20 mM Tris and 150 mM NaCl, pH 7.5) plus trace $NaBH_4$ for 5 min. DNA was visualized using 10 μg/ml Hoechst in TBS-TX for 5 min. Coverslips were mounted onto microscope slides by using 0.5% *p*-phenylenediamine, 20 mM Tris, pH 8.8, in 90% glycerol.

Microinjection

Microinjections were performed using an IM300 microinjector (Nikon, Tokyo, Japan) with microinjector controls (Nikon/Narishige) and a TE-300 inverted microscope (Nikon). All microinjections were performed on glass coverslips placed in a 35-mm tissue culture dish covered with MEMα without phenol red, supplemented with 10% fetal calf serum, penicillin, streptomycin, L-glutamine, and 20 mM HEPES-KOH, pH 7.2. Cells were kept on a 37°C warming tray before and after microinjection. All injectate samples were diluted in IB (50 mM K-glutamate and 0.5 mM $MgCl_2$), spun at 14,000 rpm at 4°C for 15–25 min to remove particulate matter, and kept on ice for the duration of the experiment. For fluorescent MTs, X-rhodamine–labeled tubulin, prepared according to Hyman *et al.* (1991), was injected into interphase cells at a needle concentration of 2 mg/ml.

For coinjection experiments, the tip concentration of injectate was 2 mg/ml X-rhodamine tubulin and 1 mg/ml antibody (either anti-XKCM1 or control IgG). The control IgG was either a nonimmune IgG (Sigma-Aldrich) or a random IgG to another kinesin-related protein (Walczak *et al.*, 1997) for which there is no cross-reactivity in PtK2 cells neither by immunostaining nor by immunoblotting analysis (our unpublished data). For injection of antibody alone into prophase or interphase cells, either IgG control antibody or anti-XKCM1 was diluted to 1 mg/ml in IB. For injection of prophase cells, coverslips were microinjected over a period of 5 min then fixed after a 30-min incubation. All interphase cells were allowed to recover for 1–3 h after microinjection before further experimentation took place. To image MT dynamics, coverslips were mounted on glass microscope slides using double stick tape spacers and fresh complete media lacking phenol red that had been supplemented with 20 mM HEPES-KOH, pH 7.2, and 1/25 EC Oxyrase (Oxyrase, Mansfield, OH). Coverslips were sealed with VALAP (1:1:1, petroleum jelly/lanolin/paraffin).

Microscopy and Image Acquisition

Cells were imaged on a multimode time-lapse fluorescence microscope system similar to that described by Salmon *et al.* (1998). This system consists of a Nikon E-600 microscope equipped with 40×/1.0 numerical aperture (NA) Plan Apo oil, 60×/1.4 NA Plan Apo oil, and 100×/1.3 NA Plan Fluor oil objectives (Nikon). Digital images were collected with a Micromax 1300 Y cooled charge coupled device camera (Roper Scientific, Trenton, NJ). All cameras, shutters, and filter wheels were controlled by MetaMorph software (Universal Imaging, Downington, PA). For mitotic cells, Z-series optical sections through each cell were obtained at 0.1-μm steps with the use of MetaMorph software and a stepping motor (Prior Scientific, Rockland, MA). For MT dynamics imaging, specimens were maintained at 35.5–37°C by using a 400 ASI air stream incubator (Nevtek, Burnsville, VA). Images were collected at 7-s time intervals for 5 min as described by Waterman-Storer and Salmon (1997) by using the epifluorescence setup described above with a 60×/1.4 NA Plan Apo oil objective. All time-lapse images for MT dynamics were acquired at 100-ms exposure times while focusing on the MTs in the periphery of the free edge of a cell. All micrographs were assembled in Adobe Photoshop for contrast enhancement. Montages were prepared using Canvas 5.0 or Adobe Illustrator 8.0.

Data Analysis

To determine the average fluorescence intensity within cells, digital images were collected using identical microscope settings and exposure times. All measurements were made using MetaMorph software. Individual cells were outlined using phase and soluble fluorescent protein images. This outline was digitally transferred to the exact pixel location on the corresponding MT images. The average gray scale intensity within this outline was logged and the background intensity for each image was subtracted from this number. We only measured cells absent of interfering morphological traits such as vesicular inclusions and overlapping MTs. Data were processed and plotted using Excel (Microsoft, Redmond, WA). We also used this method to measure the fluorescence intensity in transfected cells to ensure that our qualitative descriptions of GFP or GFP-XKCM1 fluorescence levels were consistent. We found that our descriptions of "low," "moderate," and "high" levels of GFP or GFP-XKCM1 expression always fell into discrete groups of pixel intensity values, showing that our qualitative assessments of overexpression levels are precise. To determine the level of excess XKCM1 in transfected PtK2 cells, 60 GFP control cells stained for endogenous KCM1 were imaged and measured as stated above to determine the baseline of KCM1 fluorescence in PtK2 cells. Sixty cells expressing GFP-XKCM1 were processed in this manner and graphed to determine the amount of excess XKCM1 at a specific level of GFP-XKCM1 expression for each transfected cell.

MT dynamics were measured as described by Waterman-Storer and Salmon (1997). Briefly, MT ends were tracked using the MetaMorph software "track points" function. All data was processed in Excel, where pixel measurements were converted to distance measurements using a 20-μm grid. Individual MT behavior was plotted as the change in distance from the origin (the starting position of the MT end) vs. time. Instantaneous growth and shortening velocities were determined by regression analyses of these plots. To determine the precision of our tracking, we tracked a MT three separate times and compared the differences between the three measurements for individual time points. This was done for three MTs to ensure that a precision within 1 μm could be achieved by our tracking methods. Changes in the position of a MT end that measured <1 μm between two consecutive time points were not counted as growth or shortening excursions, which is the same guideline used by Waterman-Storer and Salmon (1997). Pause was defined as slopes of <1 μm/min. Transition frequencies and SDs for transition frequencies were calculated for the population of MTs as described in Walker *et al.* (1988). To determine significant differences for catastrophe and rescue frequencies, means were compared using a Student's *t* test for two means with unequal variance by assuming a Poisson distribution of data (Walker *et al.*, 1988; Waterman-Storer and Salmon, 1997; Howell *et al.*, 1999), which predicts an exponential distribution of time intervals between events such as catastrophe or rescue (Pollard, 1977). This was necessary to do because some MTs in our sample sets never underwent a transition, which would not allow us to perform a standard student's *t* test on unpooled data sets. All other data values are reported as mean ± SD. To determine significant differences between means, unpaired *t* tests assuming unequal variance were performed with significant differences considered when $p < 0.05$.

RESULTS

GFP-XKCM1 Overexpression Destabilizes Microtubules in PtK2 Cells

To probe the role of XKCM1 in interphase, we transfected PtK2 cells with GFP or a GFP-XKCM1 fusion construct. The GFP-XKCM1 protein was present in a soluble pool in the cytoplasm and in the nucleus (Figure 1B), similar to the localization of the endogenous protein in *Xenopus* XL177 cells (Walczak *et al.*, 1996). GFP-XKCM1 was also localized to interphase centrosomes. To examine the effect of GFP-XKCM1 expression on the MT array, cells were fixed and processed for immunofluorescence at 48 h posttransfection. Cells expressing GFP had a morphologically normal MT array compared with neighboring cells not expressing GFP (Figure 1A); however, cells expressing moderate levels of GFP-XKCM1 had disruptions of the interphase MT array (Figure 1B), consistent with the role of XKCM1 as a MT destabilizer. Despite the significant decrease in MT polymer, there was little to no visible tubulin staining in the cytoplasm of these cells at 24–72 h posttransfection. In cells expressing high levels of GFP-XKCM1, the entire MT array was nearly abolished and a lightly staining tubulin pool was present in the cytoplasm (Figure 1C). The effects of GFP-XKCM1 overexpression were similar from 24 to 72 h posttransfection, although the overall level of expression increased with time. To determine the likelihood of MT destabilization due to GFP-XKCM1 overexpression, we examined cells expressing moderate levels of GFP or GFP-XKCM1 and then asked whether the MT arrays were destabilized at 48 h posttransfection. We found that 74% of cells

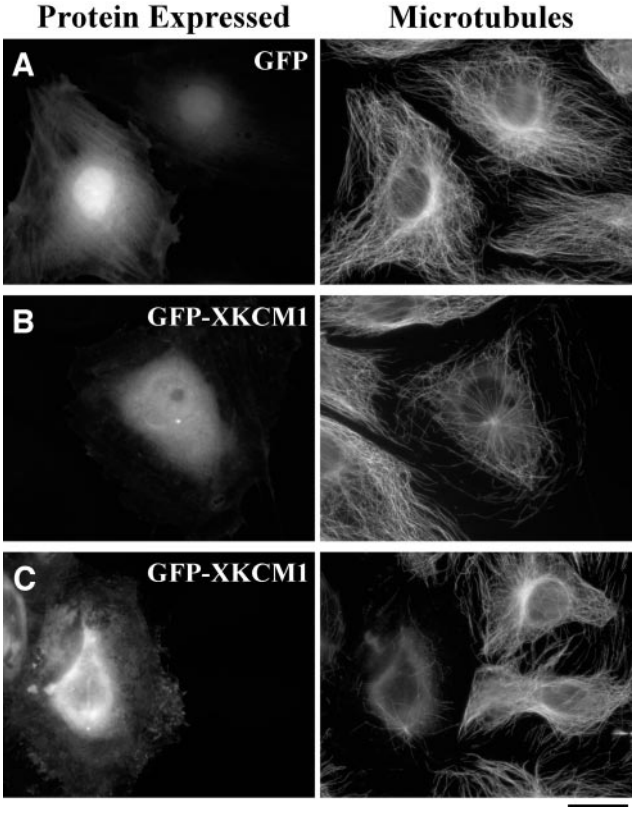

Figure 1. GFP-XKCM1 overexpression destabilizes microtubules in PtK2 cells. Cells were transfected with GFP or GFP-XKCM1 then fixed and processed for immunofluorescence at 48 h posttransfection. Digital images were taken using identical microscope settings and exposure times. (A) Control cells expressing GFP and corresponding interphase MT arrays. (B) Cell expressing a low level of GFP-XKCM1 and corresponding MT array. Note the nonexpressing cells with normal MT arrays to the left. (C) Cell expressing a high level of GFP-XKCM1 and corresponding MT array. Bar, 20 μm.

expressing moderate levels of GFP-XKCM1 had destabilized MT arrays (n = 414), whereas only 5% of cells expressing moderate levels of GFP showed a decrease in MT density (n = 500). We verified that our qualitative descriptions of low, moderate, and high levels of fluorescence intensities accurately represented discrete groups of GFP- or GFP-XKCM1–expressing cells by measuring the pixel intensity values from digital images of cells as stated in MATERIALS AND METHODS.

We also tested whether the effects of GFP-XKCM1 overexpression were unique to PtK2 cells, or whether this fusion protein could alter MT morphology in other cell types. GFP-XKCM1 overexpression destabilized MTs in HeLa cells similarly to PtK2 cells, although HeLa cells exhibited a brightly staining tubulin pool upon destabilization of MTs by GFP-XKCM1 overexpression (our unpublished data). In addition, the small, round morphology of HeLa cells made the overall effect of excess XKCM1 on MTs more difficult to visualize than in PtK2 cells. We also found that GFP-XKCM1 overexpression destabilized the MT array in *Xenopus* A6 cells (our unpublished data), but low transfection efficiency and poor MT morphology of this cell line led us to pursue our studies in the PtK2 cell line due to their nice morphology, a slightly higher transfection efficiency (10–15%), and well-characterized MT dynamics and mitotic properties.

Increased Overexpression of GFP-XKCM1 Decreases the Level of Microtubule Staining

We observed that the extent of MT destabilization was tightly correlated with the level of GFP-XKCM1 expression. To quantify this effect, we collected digital images of PtK2 cells that had been fixed and processed for immunofluorescence of MTs at 48 h posttransfection. We then measured the average intensities of both the immunostained MTs (Texas Red channel) and the GFP or GFP-XKCM1 fluorescence (fluorescein isothiocyanate [FITC] channel) within individual cells. Because there was little to no tubulin pool staining in cells with GFP-XKCM1–induced destabilization of MTs, the Texas Red fluorescence intensity measurements could be used to estimate MT polymer levels. Cells expressing GFP had a broad range of MT staining that exhibited no correlation to the level of GFP expression (Figure 2A). In striking contrast, cells overexpressing GFP-XKCM1 showed a steep decrease in MT staining as the level of GFP-XKCM1 increased (Figure 2B). This eventually leveled off to a point we termed "maximal destabilization," beyond which additional GFP-XKCM1 had little effect on the MT array. The residual fluorescence in these cells was due to the soluble tubulin pool and a few remaining MTs.

To determine how much overexpression of GFP-XKCM1 was required to reach maximal destabilization of cellular MTs, in which the MT array was nearly obliterated, we stained transfected cells with an antibody raised against the N terminus of XKCM1 (Walczak *et al.*, 1996) to compare the levels of the expressed protein. Immunoblot analysis of *Xenopus* XL177 cell extracts and PtK2 cell extracts indicated that this antibody recognized the endogenous KCM1 protein in PtK2 cells with a similar affinity as XKCM1 in XL177 cells, and both cell lines exhibited an identical staining pattern when processed for immunofluorescence by using the anti-XKCM1 antibody (data not shown). By staining transfected PtK2 cells with this antibody, we found that maximal destabilization of cellular MTs was achieved at 10–20-fold excess expression of GFP-XKCM1 over endogenous levels of the protein in PtK2 cells. These results lead us to conclude that increased levels of XKCM1 expression lead to an increase in the extent of MT destabilization in somatic cells.

Overexpression of GFP-XKCM1 Prevents Incorporation of Injected Labeled Tubulin into Microtubule Arrays

We next wanted to measure individual MT dynamics in cells overexpressing GFP-XKCM1. We microinjected X-rhodamine–labeled tubulin into cells at 48 h posttransfection and examined the MT array 1–3 h postinjection. Cells expressing GFP alone incorporated rhodamine tubulin into their interphase MT arrays similarly to neighboring cells not expressing GFP (data not shown; n = 37). In contrast, 88% of cells overexpressing GFP-XKCM1 did not incorporate injected rhodamine tubulin into their MT arrays and instead had a bright pool of fluorescent tubulin in the cytoplasm at 1–3 h postinjection (data not shown; n = 40). Due to the high

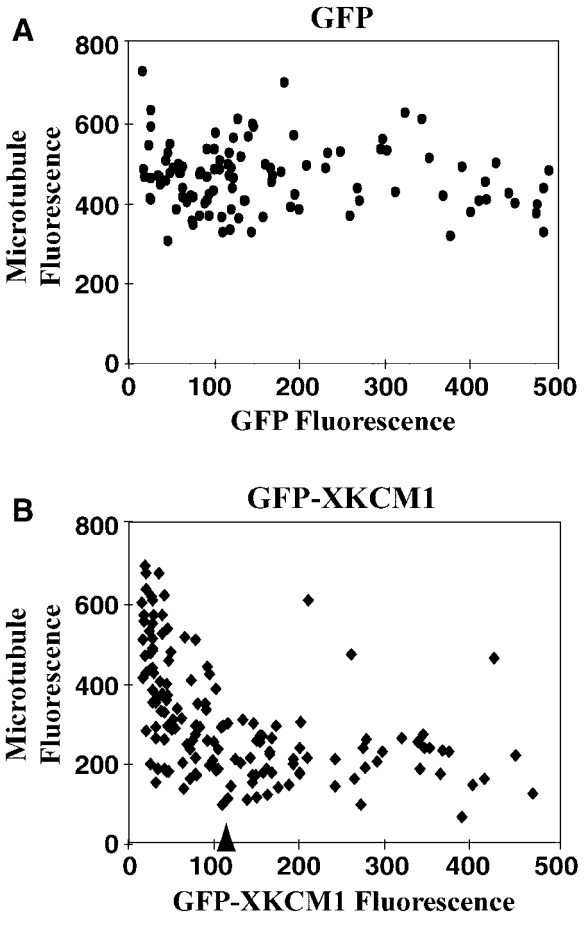

Figure 2. Increased overexpression of GFP-XKCM1 decreases the level of microtubule polymer. The average pixel intensities in both the fluorescein channel (GFP or GFP-XKCM1) and the Texas Red channel (MTs) were measured for each cell and then plotted as a single point on the graphs. (A) Plot of cells expressing different levels of GFP (n = 107 cells). (B) Plot of cells expressing different levels of GFP-XKCM1 (n = 164 cells). The arrow indicates the level of GFP-XKCM1 intensity at which "maximal destabilization" of MTs occurred.

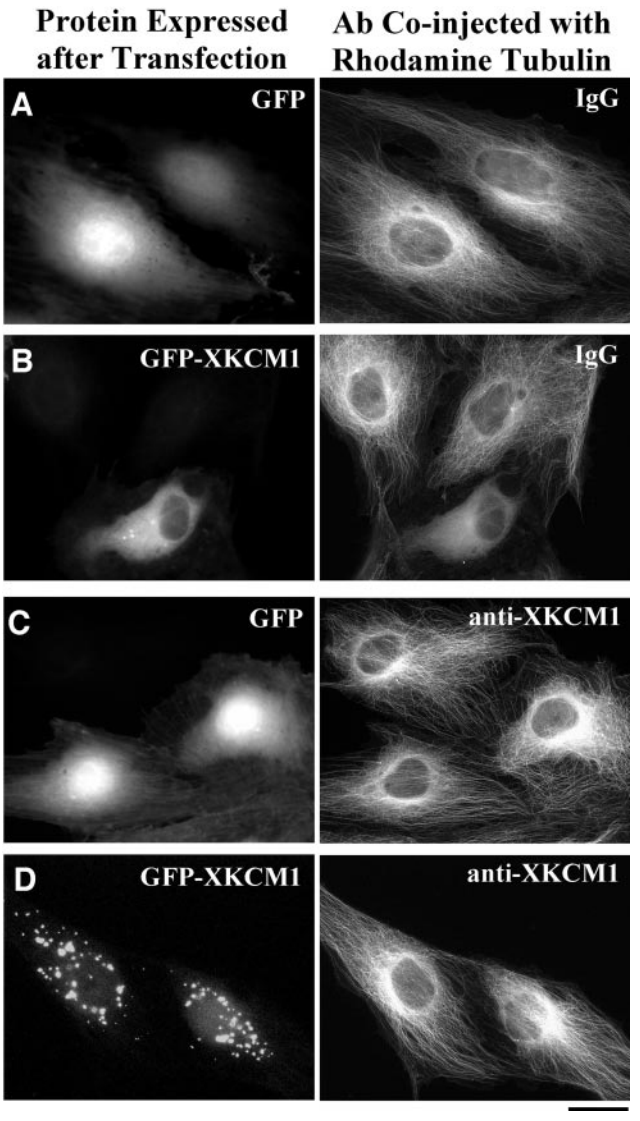

Figure 3. Inhibitory anti-XKCM1 antibody rescues the effect of GFP-XKCM1 overexpression. PtK2 cells were transfected with either GFP or GFP-XKCM1 and coinjected with antibody plus X-rhodamine tubulin at 48 h posttransfection. Cells were then fixed at 1–3 h postinjection. (A) Cells expressing GFP coinjected with labeled tubulin and random IgG antibody. (B) Cell expressing GFP-XKCM1 and coinjected with labeled tubulin and a random IgG antibody. Note soluble tubulin pool in cell expressing GFP-XKCM1 vs. normal MT arrays in two nonexpressing cells. (C) Cells expressing GFP and coinjected with inhibitory anti-XKCM1 antibody and labeled tubulin. (D) Cells expressing GFP-XKCM1 and coinjected with labeled tubulin and inhibitory anti-XKCM1 antibody. Note cytoplasmic aggregations of GFP-XKCM1 and corresponding normal interphase arrays. Bar, 20 μm.

background fluorescence of tubulin subunits in the cytoplasm, the 12% of cells overexpressing GFP-XKCM1 that did incorporate injected rhodamine tubulin into MTs could not be imaged to measure individual MT behavior.

To test whether the lack of incorporation of rhodamine tubulin into MTs was due to overexpression of GFP-XKCM1, we analyzed the MT array at 1–3 h after coinjecting a mixture of either X-rhodamine tubulin and a random IgG antibody or X-rhodamine tubulin and the anti-XKCM1 antibody described above, which inhibits XKCM1 activity in egg extracts (Walczak *et al.*, 1996; Tournebize *et al.*, 2000). If the excess XKCM1 was preventing injected tubulin incorporation then its inhibition would rescue this defect. Control cells expressing GFP alone that were coinjected with a mixture of random IgG and rhodamine tubulin had morphologically normal MT arrays (Figure 3A; n = 32), whereas 85% of cells expressing GFP-XKCM1 that were coinjected with a random IgG and rhodamine tubulin had bright pools of unpolymerized fluorescent tubulin subunits (Figure 3B; n = 40). Cells expressing GFP alone that were coinjected with anti-XKCM1 antibody and labeled tubulin had morphologically normal arrays, although they often exhibited an in-

crease in the density of MTs in the perinuclear region (Figure 3C; n = 21). Consistent with the hypothesis that excess XKCM1 was preventing polymerization of injected tubulin, microinjection of inhibitory anti-XKCM1 antibody restored the MT array morphology and density to that of control cells in 42% of cells overexpressing GFP-XKCM1 (Figure 3D; n = 50). The probability of rescue depended on the level of GFP-XKCM1 expression, with the cells expressing the highest levels of GFP-XKCM1 still exhibiting bright tubulin pools and no MTs that could be visualized by fluorescence microscopy. In addition, cells injected with inhibitory antibody often exhibited aggregates of GFP-XKCM1 protein in the cytoplasm (Figure 3D), which were never seen in cells expressing GFP-XKCM1 that were uninjected or injected with random IgG (Figure 3B). These results lead us to conclude that the lack of incorporation of injected labeled tubulin is a consequence of GFP-XKCM1 overexpression.

Overexpression of GFP-XKCM1 Increases the Catastrophe Frequency and Decreases the Rescue Frequency of Microtubules

We reasoned that at earlier time points after transfection, cells might express sufficiently low levels of GFP-XKCM1 to allow for incorporation of rhodamine tubulin into the MT array and subsequent visualization of the MTs. In an effort to measure MT dynamics, we microinjected X-rhodamine–labeled tubulin at 24 h posttransfection into cells expressing low levels of GFP-XKCM1. By measuring the fluorescence intensity in immunostained GFP-XKCM1–expressing cells as in Figure 2, we found that the cells microinjected at 24 h posttransfection expressed only 4–6-fold excess XKCM1 relative to the endogenous level of KCM1 in PtK2 cells. At this level of GFP-XKCM1 expression, cells did not exhibit gross changes in MT array morphology. This allowed us to visualize MTs in many of the cells we examined. At 1–3 h postinjection, MTs in the cell periphery at the free edge of a cell were imaged using time-lapse fluorescence microscopy (Figure 4, A–D) and individual MT dynamics were measured (Figure 4, E and F). We analyzed MTs that could be visualized for at least half of the 5-min imaging period, and MTs in a continuous state of pause were not included in our data sets. In addition, to restrict our sampling to MT plus ends, we only analyzed MTs that extended back toward the centrosome as far as it was possible to visualize by fluorescence microscopy. Although we observed many free MTs in the cytoplasm of cells overexpressing GFP-XKCM1, these MTs were never included in our data sets for MT dynamics measurements. Most of these MTs were parallel to the cell edge and often moved through the cytoplasm initially then depolymerized rapidly and completely from the trailing end of the MT to the tip (our unpublished data).

The parameters of MT dynamic instability were measured and compared between cells expressing GFP or GFP-XKCM1 by using the MT dynamics conventions set forth by Walker *et al.* (1988). In cells expressing low levels of GFP-XKCM1, we found a 4.5-fold increase in the MT catastrophe frequency ($p < 0.001$) and a 1.7-fold decrease in the MT rescue frequency ($p < 0.05$) compared with GFP control cells (Table 1). In addition, the growth rate increased 1.7-fold ($p < 0.001$), whereas the shrinkage rate decreased 1.4-fold ($p < 0.05$) in cells expressing GFP-XKCM1.

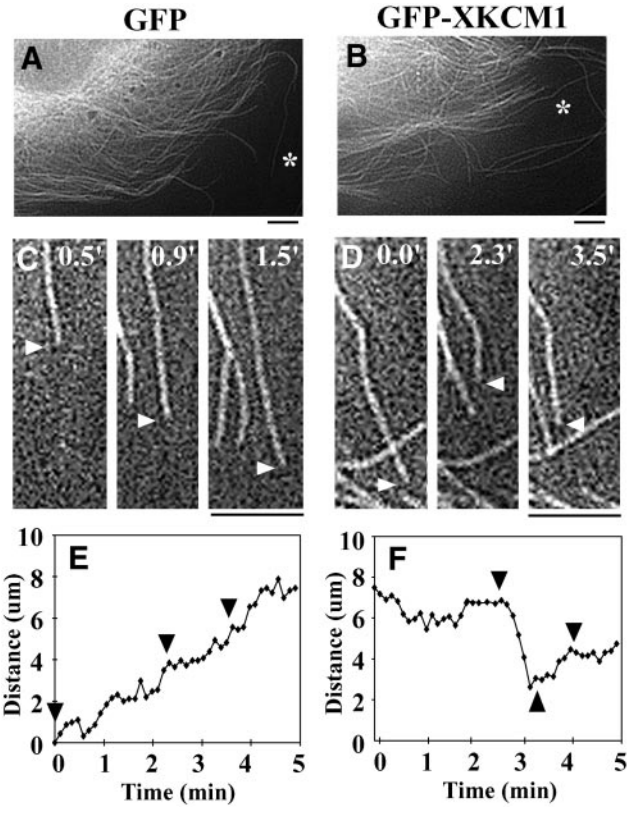

Figure 4. Overexpression of GFP-XKCM1 increases dynamic instability of microtubules. PtK2 cells were transfected with GFP or GFP-XKCM1 and microinjected with labeled tubulin at 24 h posttransfection. Individual MTs were visualized in live cells at 1–3 h posttransfection. Rhodamine MTs in representative cells expressing GFP (A) or GFP-XKCM1 (B). Asterisks lie next to the MTs represented in C–F. Individual MTs in live cells expressing either GFP (C) or GFP-XKCM1 (D) were imaged for MT dynamics. Actual image times are in the top right corner. White arrowheads denote the end of the MT. (E) Life history plot of the MT shown in C in a cell expressing GFP. Black arrowheads correspond to the three image time points. (F) Life history plot of the MT shown in D in a cell expressing GFP-XKCM1. Black arrowheads correspond to the three image time points. Bars, 5 μm.

There were three additional differences between GFP control cells and cells expressing GFP-XKCM1 that were consistent with overexpression of a MT-destabilizing protein. First, MTs in control cells spent only 7% of their cumulative lifetime in a state of shrinkage, whereas MTs in cells expressing GFP-XKCM1 spent 29% of their lifetime shrinking (Table 1). Second, there was a 17.7-fold decrease in the number of MTs that never shrank in cells expressing GFP-XKCM1 compared with control cells. Third, although every MT in cells expressing GFP underwent growth excursions, 13% of the MTs in cells overexpressing GFP-XKCM1 never grew.

We were surprised to find that MTs in control cells expressing GFP alone were not very dynamic compared with the published values for MT dynamics in PtK1 cells (Shelden and Wadsworth, 1993). To determine whether the diminished dynamics of MTs in GFP-expressing cells were due to the reagents used in the transfection procedure, we mea-

Table 1. Overexpression of GFP-XKCM1 increases dynamic instability in PtK2 cells

	Nonexpressing transfected cells	GFP-expressing cells	GFP-XKCM1-expressing cells
Catastrophe frequency (s^{-1}) (± SD)	0.0036 (±0.0009)	0.0039 (±0.0009)	0.0177 (±0.0023)
Rescue frequency (s^{-1}) (± SD)	0.0286 (±0.0074)	0.0357 (±0.0087)	0.0212 (±0.0031)
Growth rate (μm/min) (± SD)	4.5 (±3.8)	3.6 (±2.4)	6.0 (±4.9)
Shrinkage rate (μm/min) (± SD)	10.9 (±6.4)	9.5 (±5.6)	6.9 (±5.0)
% Time growing (± SD)	52.0 (±26.8)	66.2 (±27.6)	34.1 (±21.4)
% Time shrinking (± SD)	5.8 (±9.4)	7.2 (±12.3)	29.0 (±17.6)
% Time pausing (± SD)	42.2 (±23.7)	28.9 (±25.0)	38.7 (±23.3)
% MTs never shrinking	40.6	56.7	3.2
% MTs never growing	3.1	0.0	12.9
No. of MTs analyzed	32*	30	31
No. of Cells analyzed	7*	6	6

Parameters of MT dynamics were measured at the periphery of the free edge of live cells expressing GFP, GFP-XKCM1, or no transfection construct ("nonexpressing" cells) as described in MATERIALS AND METHODS.

* Nonexpressing cell sample sizes are divided as follows: 15/32 MTs imaged were from three cells on coverslips with cells expressing GFP; 17/32 MTs imaged were from four cells on coverslips with cells expressing GFP-XKCM1.

sured individual MT dynamics of cells that were exposed to the transfection reagents but were not expressing a transfection construct. These cells, called "nonexpressing" cells, were on coverslips that were transfected with either GFP or GFP-XKCM1 constructs. We analyzed the two types of nonexpressing cells both separately and as a group, and found no statistically significant differences between nonexpressing cells and GFP-expressing cells (Table 1). This suggests that the decreased dynamics seen in cells expressing GFP alone resulted from the $CaPO_4$ transfection procedure itself and not from the expression of GFP. Overall, these findings suggest the destabilization of MTs in cells overexpressing GFP-XKCM1 is due to an increase in the catastrophe frequency and a decrease in the rescue frequency of MTs.

Injection of Inhibitory Anti-XKCM1 Antibody Increases Microtubule Density in PtK2 Cells

To complement our studies of GFP-XKCM1 overexpression, we wanted to examine the effect of KCM1 inhibition in PtK2 cells. We microinjected inhibitory antibodies into interphase PtK2 cells and processed the cells for immunofluorescence of MTs and injected primary antibodies at 1–3 h after microinjection. We found that cells injected with anti-XKCM1 antibody exhibited an increase in the density of MTs in the perinuclear region of the cell compared with control IgG-injected cells or uninjected neighboring cells (Figure 5, A and B). This effect was also observed upon coinjection of anti-XKCM1 antibody and labeled tubulin into cells expressing GFP or GFP-XKCM1 (Figure 3, C and D).

To measure the level of MT fluorescence when KCM1 is inhibited, we collected digital images of PtK2 cells that had been fixed and processed for immunofluorescence of injected antibodies and MTs at 1–3 h after microinjection. We then measured the average fluorescence intensity of MTs in the injected cells. We found that inhibitory anti-XKCM1 antibody injection increased the fluorescence of MTs by 14% over IgG-injected controls ($p < 0.001$; $n = 95$ IgG-injected cells and 98 anti-XKCM1-injected cells). These findings demonstrate that KCM1 inhibition in PtK2 cells leads to an increase in the level of MT staining.

Inhibition of KCM1 Decreases the Catastrophe Frequency and Increases the Rescue Frequency of Microtubules in PtK2 Cells

To determine how the parameters of dynamic instability were altered in cells injected with an inhibitory anti-XKCM1

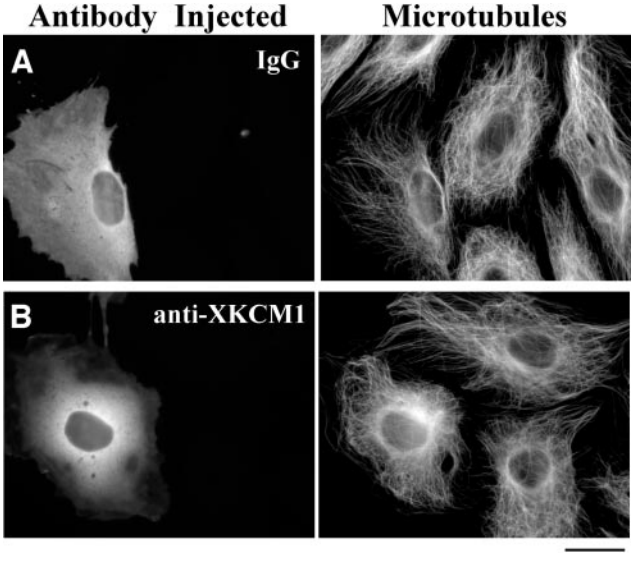

Figure 5. Injection of inhibitory anti-XKCM1 antibody increases microtubule density. PtK2 cells were microinjected with antibody and fixed and processed for immunofluorescence at 1–3 h postinjection. (A) Cell injected with nonimmune IgG antibody and corresponding MT array. Note similar MT arrays of uninjected cells. (B) Cell injected with inhibitory anti-XKCM1 antibody and corresponding MT array. Note slight increase in density of perinuclear MTs in injected cells compared with uninjected cells to the right. Bar, 20 μm.

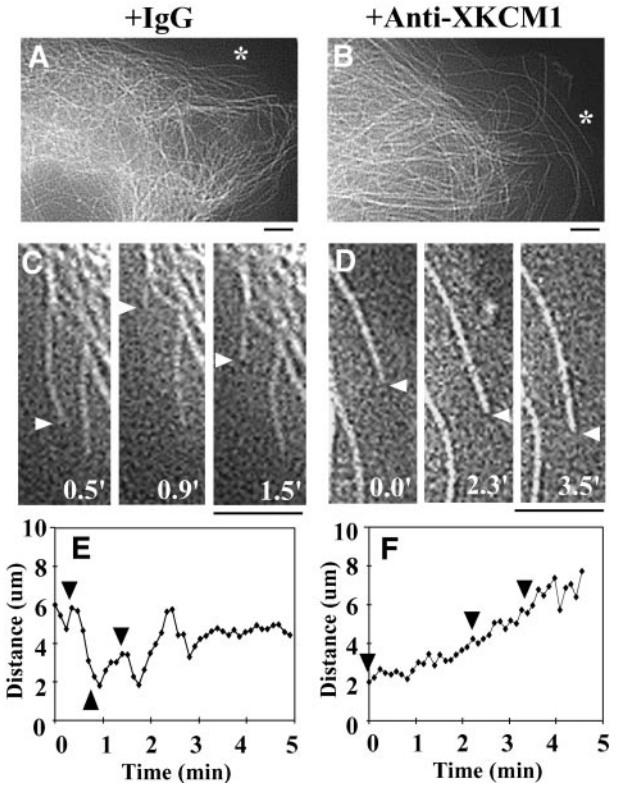

Figure 6. Inhibition of KCM1 suppresses dynamic instability of microtubules. PtK2 cells were coinjected with antibody and rhodamine-labeled tubulin. Individual MTs were visualized in live cells at 1–3 h posttransfection. Rhodamine MTs in representative cells injected with nonimmune IgG antibody (A) or inhibitory anti-XKCM1 antibody (B). The asterisks lie next to the MTs represented in C–F. Individual MTs in live cells injected with either IgG antibody (C) or inhibitory anti-XKCM1 antibody (D) were imaged for MT dynamics. Actual image times are in the bottom right corner. White arrowheads denote the end of the MT. (E) Life history plot of the MT shown in C in a cell injected with control IgG. Black arrowheads correspond to the three image time points. (F) Life history plot of the MT shown in D in a cell injected with anti-XKCM1 antibody. Black arrowheads correspond to the three image time points. Bars, 5 μm.

antibody, we coinjected cells with a mixture of either nonimmune IgG and rhodamine tubulin or anti-XKCM1 antibody and rhodamine tubulin to examine the behavior of individual MTs. At 1–3 h postinjection, MTs in the cell periphery at the free edge of a cell were imaged using time-lapse fluorescence microscopy (Figure 6, A–D), and individual MT dynamics were measured (Figure 6, E and F).

In cells coinjected with the inhibitory anti-XKCM1 antibody and labeled tubulin, there was a 2.1-fold decrease in the MT catastrophe frequency ($p < 0.01$) and a 1.9-fold increase in the MT rescue frequency ($p < 0.01$) compared with nonimmune IgG-injected cells (Table 2). Consistent with this finding, MTs spent 2.6-fold less time in a state of shrinkage, and there was a 5.3-fold increase in the number of MTs that never underwent shrinkage when KCM1 was inhibited. In addition, although 17% of MTs in IgG-injected control cells never grew, we found that every MT in anti-XKCM1-injected cells exhibited growth excursions (Table 2). Inhibition of KCM1 also caused a 1.6-fold increase in the shrinkage rate of MTs in injected cells ($p < 0.001$). These findings suggest that the increase in MT staining upon KCM1 inhibition in PtK2 cells is due to a decrease in the catastrophe frequency and an increase in the rescue frequency of MTs.

Altering the Level of XKCM1 during Mitosis Affects Spindle Morphology

We next sought to address what would happen if cells overexpressing GFP-XKCM1 entered mitosis. In control cells GFP was localized in a soluble pool (Figure 7A). Consistent with XKCM1 staining in XL177 cells (Walczak *et al.*, 1996), GFP-XKCM1 was present in a soluble pool and localized to poles and centromeres in mitotic cells (Figure 7, B–D). In cells expressing GFP and in nonexpressing transfected cells, the mitotic index was ~2% (n = 1000 nonexpressing and 992 GFP-expressing cells). In contrast, ~6% of cells expressing GFP-XKCM1 were mitotic (n = 310), suggesting that cells overexpressing GFP-XKCM1 exhibited a mitotic arrest or a mitotic delay.

Consistent with this finding, 62% of mitotic cells expressing GFP-XKCM1 had abnormal spindles compared with cells expressing GFP or to nonexpressing control cells (n =

Table 2. Inhibition of KCM1 suppresses dynamic instability in PtK2 cells

	IgG-injected cells	Anti-XKCM1-injected cells
Catastrophe frequency (s^{-1}) (± SD)	0.0116 (±0.0018)	0.0056 (±0.0010)
Rescue frequency (s^{-1}) (± SD)	0.0203 (±0.0031)	0.0378 (±0.0073)
Growth rate (μm/min) (± SD)	4.8 (±3.9)	4.0 (±2.1)
Shrinkage rate (μm/min) (± SD)	6.4 (±4.3)	10.0 (±5.5)
% Time growing (± SD)	38.7 (±27.0)	63.8 (±24.4)
% Time shrinking (± SD)	19.9 (±17.3)	7.6 (±10.5)
% Time pausing (± SD)	39.4 (±22.9)	29.0 (±22.5)
% MTs never shrinking	8.6	45.9
% MTs never growing	17.1	0.0
No. of MTs analyzed	35	37
No. of Cells analyzed	6	8

Parameters of MT dynamics were measured at the periphery of the free edge of live cells injected with either nonimmune IgG or inhibitory anti-XKCM1 antibody as described in MATERIALS AND METHODS.

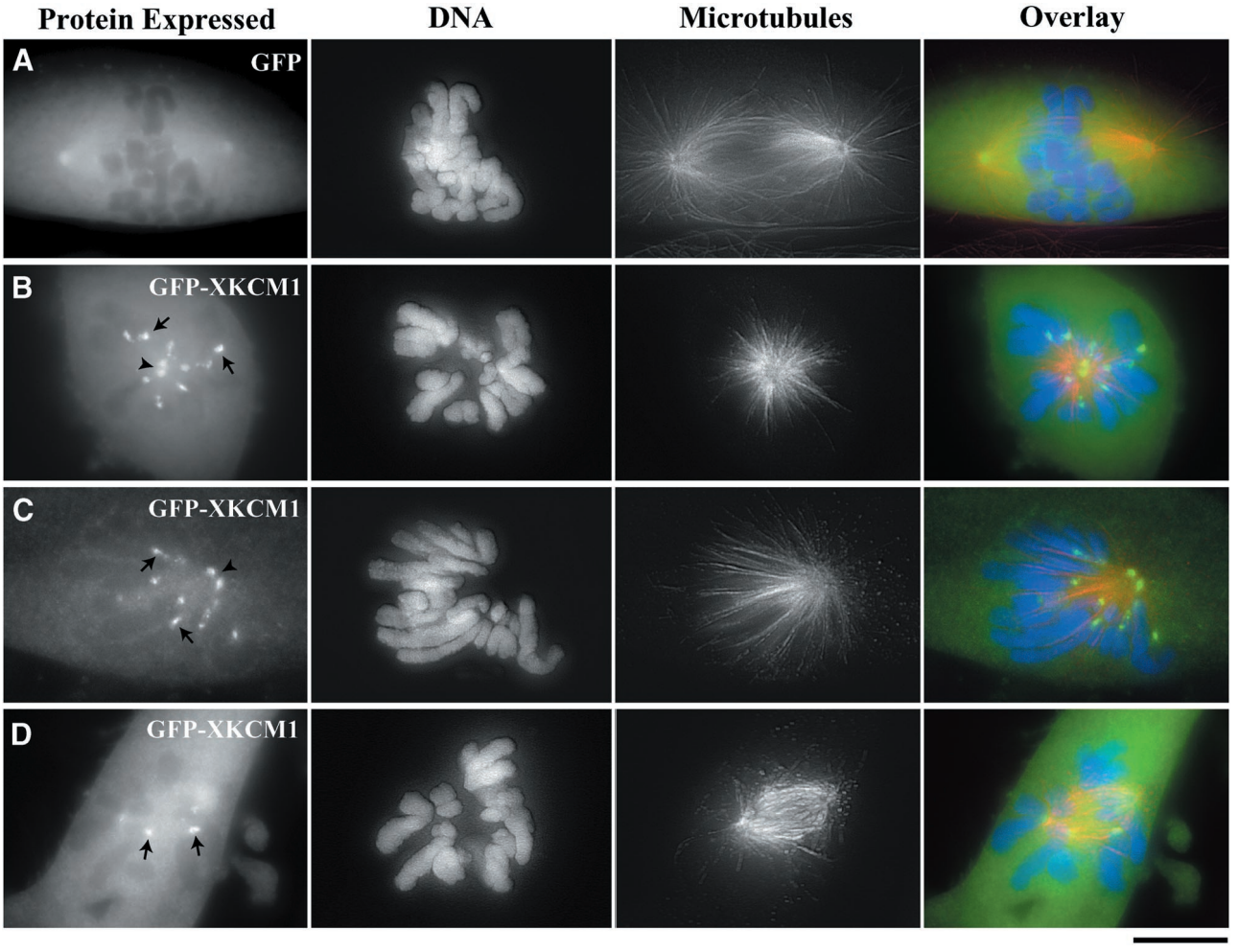

Figure 7. Overexpression of GFP-XKCM1 perturbs spindle morphology in PtK2 cells. Cells were transfected with GFP or GFP-XKCM1 and processed for immunofluorescence microscopy at 72 h posttransfection. MTs are in red and DNA is in blue. Optical Z-series images were collected using a Z-axis motor and three-dimensionally reconstructed in MetaMorph. (A) Prometaphase spindle in a cell expressing GFP. (B) Monoastral spindle in a cell overexpressing GFP-XKCM1. (C) Monopolar spindle in a cell overexpressing GFP-XKCM1. (D) Prometaphase-like spindle in a cell overexpressing GFP-XKCM1. Arrowheads point between unseparated centrosomes. Arrows denote centromere localization of GFP-XKCM1. Bar, 10 μm.

63). The most frequent abnormalities included monoastral and monopolar spindles (54% of abnormal spindles; Figure 7, B and C). Monoastral spindles had two closely spaced centrosomes in the center of the cells surrounded by chromosomes, whereas monopolar cells had two closely spaced centrosomes to one side of the cell, with all of the chromosomes on the opposite side of the cell. In addition, we found many small prometaphase-like spindles with improperly attached chromosomes (31% of abnormal spindles; Figure 7D). Chromosomes in these cells were often oriented with their arms located far outside the spindle, and some chromosomes were completely unattached from the spindle and floating freely in the cytoplasm. These prometaphase-like spindles also exhibited poorly focused spindle poles and virtually no astral MTs. These findings suggest that both the formation and function of the mitotic spindle are sensitive to the increased expression of XKCM1.

We were also interested in how the inhibition of KCM1 during mitosis would affect the mitotic spindle. To examine this, we microinjected nonimmune IgG antibody or inhibitory anti-XKCM1 antibody into the cytoplasm of prophase cells. Each coverslip was injected over a period of 5 min and then fixed and processed for fluorescence of MTs, DNA and the injected antibody at 30 min postinjection. Injected cells were then analyzed to determine what stage of mitosis they had reached and whether they exhibited defects in spindle morphology. Interestingly, we found that after a 30-min incubation, 77% of cells injected with anti-XKCM1 were still in prometaphase ($n = 85$), whereas only 41% of IgG-injected cells were in prometaphase ($n = 69$; Figure 8). This 35% increase in the number of anti-XKCM1-injected cells still in prometaphase ($p < 0.01$) suggests that these cells were either delayed or arrested in mitosis. This is also reflected in the finding that there is a 20% decrease in the number of anti-

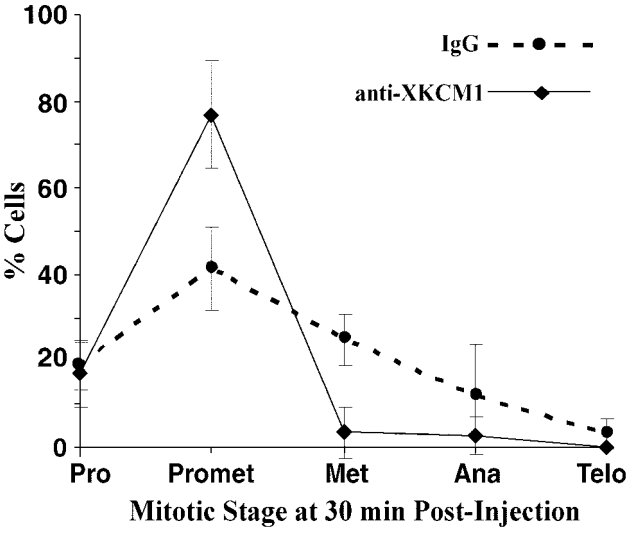

Figure 8. Inhibition of KCM1 in mitosis leads to a mitotic delay in PtK2 cells. Prophase cells were microinjected with either nonimmune IgG or inhibitory anti-XKCM1 antibody. At 30 min postinjection, cells were fixed and processed for fluorescence of injected antibodies, MTs, and DNA. The percentage of cells in each stage of mitosis was determined and plotted for IgG-injected cells (dotted line) vs. cells injected with anti-XKCM1 antibody (solid line).

XKCM1–injected mitotic cells that had reached metaphase by this time point ($p < 0.01$).

A mitotic delay or arrest is consistent with the spindle morphology defects we observed in anti-XKCM1–injected mitotic cells vs. IgG-injected mitotic cells that were fixed 30 min postinjection. Compared with IgG-injected cells in prometaphase (Figure 9A), 53% of the anti-XKCM1–injected cells exhibited spindle morphology defects consistent with the inhibition of a MT-destabilizing protein ($n = 64$). The most predominant spindle defect was a "hairy" prometaphase spindle, in which there were obvious increases in both the length and density of spindle and astral MTs (30% of all prometaphase spindles; Figure 9B). In addition, we often observed monoastral spindles with partially separated poles and many long MTs emanating radially out to the cell periphery (23% of all prometaphase spindles; Figure 9C), reminiscent of the huge MT asters found in mitotic egg extracts upon inhibition or immunodepletion of XKCM1 (Walczak *et al.*, 1996). These monoastral spindles often had all chromosomes clustered to one side. Despite the aberrant morphology of the monoastral spindles, they were classified as prometaphase because the chromosomes had not yet congressed, but nuclear envelope breakdown had occurred. This could be determined by the FITC staining pattern of the injected antibodies, which did not enter the nuclear region until after nuclear envelope breakdown (data not shown). In addition, the FITC staining pattern indicated that anti-XKCM1 antibody injection into mitotic cells blocked the ability of endogenous KCM1 protein to target to centromeres and spindle poles (Figure 9, B and C). Taken together, the observed spindle morphology defects observed upon injection of anti-XKCM1 antibody suggest that inhibition of KCM1 perturbs the formation and function of the mitotic spindle.

DISCUSSION

Previous studies showed that XKCM1 is the dominant MT destabilizer in cytoplasmic extracts prepared from *Xenopus* eggs (Walczak *et al.*, 1996; Tournebize *et al.*, 2000); however, whether XKCM1 acts as a MT destabilizer in somatic cells and the importance of its contribution to cellular MT dynamics have not been addressed. Herein, we explore the effect of XKCM1 inhibition or overexpression in PtK2 cells with live and fixed analyses of the MT cytoskeleton. We found that the MT arrays in PtK2 cells are sensitive to the level of XKCM1 expression during interphase and that altering the level of XKCM1 in mitosis leads to defects in spindle morphology. Measurements of individual MT dynamics revealed that XKCM1 perturbation causes dramatic effects on the catastrophe frequency and modest effects on the rescue frequency of MTs in PtK2 cells. These results lead us to conclude that XKCM1 is an essential regulator of MT dynamics in vertebrate somatic cells.

XKCM1 Regulates Microtubule Organization in Somatic Cells

Our findings demonstrate that XKCM1 acts as a MT destabilizer not only in vitro and in egg extracts but also in cells. Given that GFP-XKCM1 destabilized MTs in *Xenopus* A6 cells, marsupial PtK2 cells, and human HeLa cells, it is clear that the activity of this protein is conserved in vertebrate somatic cells. Previous studies in CHO cells with a GFP fusion with the hamster homolog of XKCM1, MCAK, have given variable results with respect to depolymerization. In the first study, overexpression of GFP-MCAK resulted in no effect in CHO cells at 16–24 h but did cause a decrease in MT polymer in mitotic cells at 70 h (Maney *et al.*, 1998). In contrast, a recent study reported a noticeable decrease in interphase MT staining due to GFP-MCAK overexpression at 18 h posttransfection (Maney *et al.*, 2001). The source of the differences between these two studies is not clear, although the observation that MT morphology is affected by MCAK overexpression is consistent with our findings.

We were surprised to find that PtK2 cells overexpressing GFP-XKCM1 had little to no soluble tubulin pool staining in the cytoplasm, despite the significant destabilization of MTs. One possible explanation of these results is that XKCM1 somehow modulates intracellular tubulin levels. It is more likely that the lack of cytoplasmic tubulin staining is due to autoregulation of tubulin expression, wherein tubulin transcription is suppressed in response to an increase in the level of unpolymerized tubulin subunits (Ben-Ze'ev *et al.*, 1979; Cleveland *et al.*, 1981). Consistent with this idea, we found that a 24-h nocodazole treatment also causes a diminished MT array and little tubulin pool staining in the cytoplasm of many PtK2 cells (our unpublished data). Autoregulation of tubulin levels in PtK2s could explain why microinjected fluorescent tubulin was present at such high levels in the cytoplasm of cells expressing GFP-XKCM1. The destabilizing activity of XKCM1 would not favor stable incorporation of tubulin into the MT array, and the short incubation period

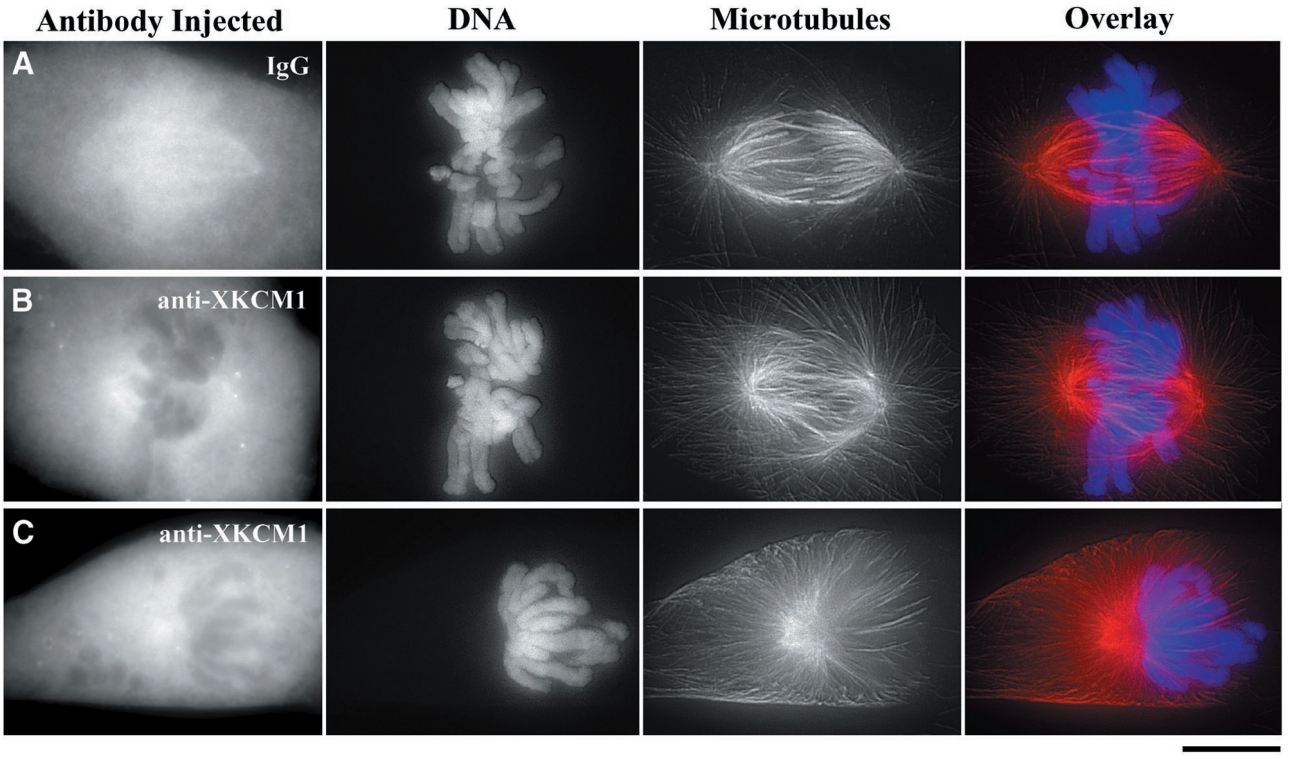

Figure 9. Inhibition of KCM1 in mitosis perturbs spindle morphology in PtK2 cells. Prophase cells were microinjected with either nonimmune IgG or inhibitory anti-XKCM1 antibody. At 30 min postinjection, cells were fixed and processed for fluorescence of injected antibodies, MTs (red), and DNA (blue). Optical Z-series images were collected using a Z-axis motor and three-dimensionally reconstructed in MetaMorph. (A) Prometaphase spindle in a cell injected with IgG. (B) Hairy prometaphase spindle in a cell injected with anti-XKCM1. (C) Monoastral spindle in a cell injected with anti-XKCM1. Note lack of XKCM1 staining at centromeres and spindle poles in B and C. Bar, 10 μm.

of 1–3 h may not be sufficient for down-regulation of tubulin expression levels.

When KCM1 was inhibited there was a small increase in MT polymer staining, which was predominantly in the perinuclear region of PtK2 cells. A similar effect is seen upon inhibition of the MT destabilizer Op18 (Howell *et al.*, 1999). An increase in MT density in this region could be due to an increase in MT nucleation, a decrease in the frequency of MT release from the centrosome (Keating *et al.*, 1997), or an increase in the stabilization of MTs near the centrosome by localized MAPs, such as TOGp (Charrasse *et al.*, 1998). Further experiments are necessary to determine whether XKCM1 plays a role in centrosomal release of MTs or in the regulation of pericentrosomal MTs organized by proteins such as cytoplasmic dynein (Vorobjev *et al.*, 2001).

Altering the level of XKCM1 was also found to affect MTs in mitotic PtK2 cells. The predominant spindle defects due to GFP-XKCM1 overexpression, including monopolar spindles, monoastral spindles, and small prometaphase-like spindles with poorly organized poles, improperly attached chromosomes, and no astral MTs, could all result from excess spindle MT destabilization. For example, monopolar and monoastral spindles could result from the failure of centrosomes to separate or from the collapse of an unstable bipolar spindle. To determine how these spindles are formed and whether they arrest in mitosis, it will be necessary to perform live analysis. Although CHO cells overexpressing GFP-MCAK exhibit a pseudoprometaphase arrest (Maney *et al.*, 1998), the spindle structures in these cells are very different from the prometaphase-like spindles we have analyzed. Specifically, we have not observed MT bundling in PtK2 cells overexpressing GFP-XKCM1. In addition, we found that more than half of the abnormal spindles in PtK2 cells were monopolar or monoastral, which were not reported in CHO cells overexpressing GFP-MCAK. Because mitotic CHO cells are able to be removed by mitotic shake-off (Maney *et al.*, 1998), it is possible that the most disrupted spindles do not remain attached to the coverslip.

Differences between MCAK studies in CHO cells and KCM1 studies in PtK2 cells were also found concerning inhibition of these proteins during mitosis. Our fixed time-point analysis indicated that KCM1 inhibition leads to a mitotic arrest or delay, with an increase in the length and density of MTs disrupting the overall spindle morphology in prometaphase cells. Antisense-induced down-regulation of MCAK in CHO cells results in lagging chromosomes during anaphase, with no effect on the timing or progression of mitosis, and no differences in MT spindle morphology. Our assay is different in that our cells are injected with inhibitory antibody during prophase and allowed only 30-min incubation before fixation. This allows us to visualize cells under very specific circumstances, with every cell having already

begun the process of mitosis. It will be interesting to determine whether the spindles with excessive MTs can complete mitosis through a prolonged prometaphase, or whether these cells arrest during mitosis. Taken together, our results suggest that altering the level of KCM1 leads to major defects in spindle assembly and function during mitosis in PtK2 cells. In addition, the predominant spindle defects we have observed in mitotic cells with excess or inhibited XKCM1 are consistent with our findings that XKCM1 regulates MT catastrophe and rescue frequencies.

XKCM1 Regulates Microtubule Transition Frequencies in Somatic Cells

Our results indicate that XKCM1 is an essential regulator of MT dynamics in PtK2 cells, most notably by modulating MT transition frequencies. Overexpression of GFP-XKCM1 caused an increase in the catastrophe frequency, whereas inhibition of XKCM1 caused a decrease in the catastrophe frequency of MTs. These findings are consistent with analyses of XKCM1 by using purified proteins and in *Xenopus* egg extracts, which indicate that XKCM1 is a modulator of MT catastrophe (Walczak *et al.*, 1996; Desai *et al.*, 1999; Tournebize *et al.*, 2000; Kinoshita *et al.*, 2001). Interestingly, we also found that GFP-XKCM1 overexpression caused a decrease in the rescue frequency of MTs, whereas inhibition of XKCM1 caused an increase in the rescue frequency of MTs. An effect on rescue frequency was not previously observed in experiments in egg extracts (Walczak *et al.*, 1996; Tournebize *et al.*, 2000) and may reflect differences in the complements of MT-regulating proteins between egg extracts and somatic cells.

Additional support for this idea comes from MT dynamics studies comparing interphase and mitosis in both systems. Studies in *Xenopus* egg extracts have demonstrated that the increase in MT turnover during mitosis is predominantly due to an increase in the catastrophe frequency of MTs (Belmont *et al.*, 1990; Verde *et al.*, 1992). In contrast, a recent study in somatic cells has shown that both an increase in the catastrophe frequency and a decrease in the rescue frequency of MTs are responsible for enhancing the dynamics of astral MTs in mitosis (Rusan *et al.*, 2001). In combination with previous studies of XKCM1, we have demonstrated that the same molecule can be used in both extracts and cells to increase global MT turnover upon entry into mitosis, despite differences in how the transition frequencies are regulated in these two systems.

Another interesting observation was that the effects on MT dynamics were much greater in magnitude when overexpressing GFP-XKCM1 than when inhibiting KCM1 in interphase PtK2 cells. This was also true when examining the interphase MT array by fluorescence microscopy. What might explain these differences? First, it is possible that our inhibitory antibody does not recognize the PtK2 protein as well as the *Xenopus* protein. We think this is unlikely because immunoblotting and immunostaining indicates that the antibody recognizes both proteins equally well. An alternative idea is that XKCM1 activity in interphase cells is normally antagonized by the presence of MAPs bound to the MTs. Inhibition of XKCM1 would therefore not cause a great effect. In contrast, overexpression of XKCM1 would favor depolymerization because cells are not expressing the level of antagonistic MT-stabilizing proteins necessary to overcome excess XKCM1. This idea is supported by studies of XKCM1 and XMAP215 in egg extracts, which showed that XKCM1 and XMAP215 activities are antagonistic both in interphase and in mitotic extracts (Tournebize *et al.*, 2000). In addition, studies in the yeast *Saccharomyces cerevisiae* have shown that the MT-stabilizing protein Stu2p, a homolog of XMAP215, is counterbalanced during anaphase spindle elongation by the kinesin-related protein Kip3p, a putative MT destabilizer (Severin *et al.*, 2001). Taken together, these results support the idea that many cell types use antagonizing activities to control cytoskeletal organization. It will be interesting to examine the relationship between KCM1 and MAPs such as TOGp, the mammalian homolog of XMAP215 (Charrasse *et al.*, 1998), in somatic cells such as PtK2s.

Unlike previous studies in *Xenopus* egg extracts, we found that alterations in the levels of XKCM1 affected MT growth and shrinkage rates. Specifically, overexpression of GFP-XKCM1 resulted in an increase in growth rate and a decrease in shrinkage rate. One possible explanation for these results is that our measurements inadvertently included MTs that were not anchored at the centrosome or in the pericentrosomal material. Although we only analyzed MTs that extended as far back toward the centrosome as it was possible to visualize by fluorescence microscopy, the high density of MTs near the centrosomes of PtK2 cells made it difficult to determine whether each MT was truly anchored. If some MTs in our dynamics data sets were not anchored and were undetectably moving toward the cell periphery, this rate of motion would add to the net growth rate and detract from the net shrinkage rate of MTs affected by GFP-XKCM1. Consistent with this idea, we observed an increased number of free MTs in the cytoplasm of cells overexpressing GFP-XKCM1 compared with cells expressing GFP. It is not currently known whether these free MTs were formed by release from centrosomes (Keating *et al.*, 1997), breakage due to buckling (Waterman-Storer and Salmon, 1997), or whether they formed de novo in the cytoplasm (Vorobjev *et al.*, 1997; Yvon and Wadsworth, 1997).

Contribution of XKCM1 to Microtubule Dynamics Regulation in Interphase and Mitotic Cells

Our findings lead us to propose the following speculative model for regulation of cellular MT dynamics by XKCM1. XKCM1 is active in interphase cells, but its effect is suppressed by the stabilizing activity of MAPs. Other destabilizers, such as Op18, also contribute to the dynamics of the interphase MT array to account for the 10–20-fold increase in catastrophe in vivo compared with solutions of pure tubulin (Cassimeris *et al.*, 1988; Simon *et al.*, 1992), because Op 18 inhibition decreases the catastrophe frequency 2.5–3-fold in newt lung epithelial cells (Howell *et al.*, 1999).

On entry into mitosis, there is a sudden increase in MT turnover (Salmon *et al.*, 1984; Saxton *et al.*, 1984; Zhai *et al.*, 1996). Specifically, in cultured cells the MT catastrophe frequency doubles and the MT rescue frequency decreases nearly 4-fold during mitosis (Rusan *et al.*, 2001). Concurrent with this increase in MT turnover, the stabilizing activity of MAPs and the destabilizing activity of Op18 are both decreased by phosphorylation (for review, see Cassimeris and Spittle, 2001). This would allow the catastrophe-promoting activity of XKCM1 to predominate as the cell transits into mitosis. The increase in dynamics at this transition enables

the cell to rapidly reduce the length of interphase MTs and increase their dynamic behavior, thereby promoting spindle formation and allowing MTs to efficiently "search and capture" the kinetochores on chromosomes (for review, see Rieder and Salmon, 1998).

ACKNOWLEDGMENTS

We thank Frank McNally for transfection advice; Lynne Cassimeris and Dave Odde for help with MT dynamics statistics; Clare Waterman-Storer and Wendy Salmon for help with tubulin microinjection and MT dynamics measurements; and Arshad Desai, Stephanie Ems-McClung, and Jane Stout for comments on the manuscript. In addition, we thank Bob Silver and Eric Shelden for instruction through the Microinjection Techniques in Cell Biology course at the Marine Biological Laboratory at Woodshole, MA. This work was supported by an AHA predoctoral grant (to S.K.S.) and National Institutes of Health grant GM-59618 (to C.E.W.). C.E.W. is a scholar of the Leukemia and Lymphoma Society.

REFERENCES

Andersen, S.S.L. (2000). Spindle assembly and the art of regulating microtubule dynamics by MAPS and Stathmin/Op18. Trends Cell Biol. *10*, 261–267.

Belmont, L.D., Hyman, A.A., Sawin, K.E., and Mitchison, T.J. (1990). Real-time visualization of cell cycle dependent changes in microtubule dynamics in cytoplasmic extracts. Cell. *62*, 579–589.

Ben-Ze'ev, A., Farmer, S.R., and Penman, S. (1979). Mechanisms of regulating tubulin synthesis in cultured mammalian cells. Cell. *17*, 319–325.

Cassimeris, L., Pryer, N.K., and Salmon, E.D. (1988). Real-time observations of microtubule dynamic instability in living cells. J. Cell Biol. *107*, 2223–2231.

Charrasse, S., Schroeder, M., Gauthier-Rouviere, C., Ango, F., Cassimeris, L., Gard, D.L., and Larroque, C. (1998). The TOGp protein is a new human microtubule-associated protein homologous to the *Xenopus* XMAP215. J. Cell Sci. *111*, 1371–1383.

Cassimeris, L., and Spittle, C. (2001). Regulation of microtubule-associated proteins. Int. Rev. Cytol. *210*, 163–226.

Cleveland, D.W., Lopata, M.A., Sherline, P., and Kirschner, M.W. (1981). Unpolymerized tubulin modulates the level of tubulin mRNAs. Cell *25*, 537–546.

Cottingham, F.R., and Hoyt, M.A. (1997). Mitotic spindle positioning in *Saccharomyces cerevisiae* is accomplished by antagonistically acting microtubule motor proteins. J. Cell Biol. *138*, 1041–1053.

Desai, A., and Mitchison, T.J. (1997). Microtubule polymerization dynamics. Annu. Rev. Cell Dev. Biol. *13*, 83–117.

Desai, A., Verma, S., Mitchison, T.J., and Walczak, C.E. (1999). Kin I kinesins are microtubule-destabilizing enzymes. Cell *96*, 69–78.

Endow, S.A., Kang, S.J., Satterwhite, L.L., Rose, M.D., Skeen, V.P., and Salmon, E.D. (1994). Yeast Kar3 is a minus-end microtubule motor protein that destabilizes microtubules preferentially at the minus ends. EMBO J. *13*, 2708–2713.

Heald, R. (1999). A dynamic duo of microtubule modulators. Nat. Cell Biol. *2*, E11–E12.

Heald, R., McLoughlin, M., and McKeon, F. (1993). Human wee1 maintains mitotic timing by protecting the nucleus from cytoplasmically activated Cdc2 kinase. Cell *74*, 463–474.

Howell, B., Deacon, H., and Cassimeris, L. (1999). Decreasing oncoprotein 18/stathmin levels reduces microtubule catastrophes and increases microtubule polymer in vivo. J. Cell Sci. *112*, 3713–3722.

Hyman, A.A., Dreschel, D., Kellogg, D., Salser, S., Sawin, K., Steffen, P., Wordeman, L., and Mitchison, T.J. (1991). Preparation of modified tubulins. Methods Enzymol. *196*, 478–486.

Keating, T.J., Peloquin, J.G., Rodionov, V.I., Momcilovic, D., and Borisy, G.G. (1997). Microtubule release from the centrosome. Proc. Natl. Acad. Sci. USA *94*, 5078–5083.

Kinoshita, K., Arnal, I., Desai, A., Drechsel, D.N., and Hyman, A.A. (2001). Reconstitution of physiological microtubule dynamics using purified components. Science *294*, 1340–1343.

Maney, T., Hunter, A.W., Wagenbach, M., and Wordeman, L. (1998). Mitotic centromere-associated kinesin is important for anaphase chromosome segregation. J. Cell Biol. *142*, 787–801.

Maney, T., Wagenbach, M., and Wordeman, L. (2001). Molecular dissection of the microtubule depolymerizing activity of mitotic centromere-associated kinesin. J. Biol. Chem. *276*, 34753–34758.

Mitchison, T.J., and Kirschner, M.W. (1984). Dynamic instability of microtubule growth. Nature *312*, 237–242.

Pollard, J. (1977). A Handbook of Numerical and Statistical Techniques with Examples Mainly from the Life Sciences, Cambridge University Press: Cambridge, 161–163.

Rieder, C.L., and Salmon, E.D. (1998). The vertebrate cell kinetochore and its roles during mitosis. Trends Cell Biol. *8*, 310–317.

Rusan, N.M., Fagerstrom, C.J., Yvon, A.M., and Wadsworth, P. (2001). Cell cycle-dependent changes in microtubule dynamics in living cells expressing green fluorescent protein-alpha tubulin. Mol. Biol. Cell *12*, 971–980.

Salmon, E.D., Leslie, R.J., Saxton, W.M., Karow, M.L., and McIntosh, J.R. (1984). Spindle microtubule dynamics in sea urchin embryos. Analysis using fluorescence-labeled tubulin and measurements of fluorescence redistribution after laser photobleaching. J. Cell Biol. *99*, 2165–2174.

Salmon, E.D., Shaw, S.L., Waters, J., Waterman-Storer, C.M., Maddox, P.S., Yeh, E., and Bloom, K. (1998). A high-resolution multimode digital microscope system. Methods Cell Biol. *56*, 185–215.

Saxton, W.M., Stemple, D.L., Leslie, R.J., Salmon, E.D., Zavortink, M., and McIntosh, J.R. (1984). Tubulin dynamics in cultured mammalian cells. J. Cell Biol. *99*, 2175–2186.

Severin, F., Habermann, B., Huffaker, T., and Hyman, T. (2001). Stu2 promotes spindle elongation in anaphase. J. Cell Biol. *153*, 435–442.

Shelden, E., and Wadsworth, P. (1993). Observation and quantification of individual microtubule behavior in vivo: microtubule dynamics are cell-type specific. J. Cell Biol. *120*, 935–945.

Simon, J.R., Parsons, S.F., and Salmon, E.D. (1992). Buffer conditions and non-tubulin factors critically affect the microtubule dynamic instability of sea urchin egg tubulin. Cell Motil. Cytoskeleton *21*, 1–14.

Tournebize, R., Popov, A., Kinoshita, K., Ashford, A.J., Rybina, S., Pozniakovsky, A., Mayer, T.U., Walczak, C.E., Karsenti, E., and Hyman, A.A. (2000). Control of microtubule dynamics by the antagonistic activities of XMAP215 and XKCM1 in *Xenopus* egg extracts. Nat. Cell Biol. *2*, 13–19.

Verde, F., Dogterom, M., Stelzer, E., Karsenti, E., and Leibler, S. (1992). Control of microtubule dynamics and length by cyclin A- and cyclin B-dependent kinases in *Xenopus* egg extracts. J. Cell Biol. *118*, 1097–1108.

Vorobjev, I., Malikov, V., and Rodionov, V. (2001). Self-organization of a radial microtubule array by dynein-dependent nucleation of microtubules. Proc. Natl. Acad. Sci. USA *18*, 10160–10165.

Vorobjev, I.A., Svitkina, T.M., and Borisy, G.G. (1997). Cytoplasmic assembly of microtubules in cultured cells. J. Cell Sci. *110*, 2635–2645.

Walczak, C.E., Mitchison, T.J., and Desai, A. (1996). XKCM1: a *Xenopus* kinesin-related protein that regulates microtubule dynamics during mitotic spindle assembly. Cell. *84*, 37–47.

Walczak, C.E., Verma, S., and Mitchison, T.J. (1997). XCTK2, a kinesin-related protein that promotes mitotic spindle assembly in *Xenopus laevis* egg extracts. J. Cell Biol. *136*, 859–870.

Walker, R.A., O'Brien, E.T., Pryer, N.K., Sobeiro, M.F., Voter, W.A., Erickson, H.P., and Salmon, E.D. (1988). Dynamic instability of individual microtubules analyzed by video light microscopy: rate constants and transition frequencies. J. Cell Biol. *107*, 1437–1448.

Waterman-Storer, C.M., and Salmon, E.D. (1997). Actomyosin-based retrograde flow of microtubules in the lamella of migrating epithelial cells influences microtubule dynamic instability and turnover and is associated with microtubule breakage and treadmilling. J. Cell Biol. *139*, 417–434.

West, R.R., Malmstrom, T., Troxell, C.L., and McIntosh, J.R. (2001). Two related kinesins, klp5$^+$ and klp6$^+$, foster microtubule disassembly, and are required for meiosis in fission yeast. Mol. Biol. Cell. *12*, 3919–3932.

Wittmann, T., Hyman, A., and Desai, A. (2001). The spindle: a dynamic assembly of microtubules and motors. Nat. Cell Biol. *3*, E28–E34.

Yvon, A.M., and Wadsworth, P. (1997). Non-centrosomal microtubule formation and measurement of minus end microtubule dynamics in A498 cells. J. Cell Sci. *19*, 2391–2401.

Zhai, Y., Kronebusch, P.J., Simon, P.M., and Borisy, G.G. (1996). Microtubule dynamics at the G_2/M transition: abrupt breakdown of cytoplasmic microtubules at nuclear envelope breakdown and implications for spindle morphogenesis. J. Cell Biol. *135*, 201–214.